**Proceedings of ASME 2010 International Design Engineering Technical Conferences &
Computers and Information in Engineering Conference
IDETC/CIE 2010
August 15 – 18, 2010, Montreal, Quebec, Canada**

DETC2010/29081

3D FRACTALS FROM PERIODIC SURFACES

Yan Wang
Woodruff School of Mechanical Engineering
Georgia Institute of Technology
Atlanta, GA 30332

ABSTRACT

Fractals are ubiquitous as in natural objects and have been applied in designing porous structures such as micro antenna and porous silicon. The seemingly complex and irregular structures can be generated based on simple principles. In this paper, we present three approaches to construct 3D fractal geometries using a recently proposed periodic surface model. By applying iterated function systems to the implicit surface model in the Euclidean or parameter space, 3D fractals can be constructed efficiently. Porosity is also proposed as a metric in fractal design.

1. INTRODUCTION

Among many forms of geometries, fractals exhibit a large extent of symmetry and generalization. They are ubiquitous as in natural objects, such as trees, rocks, fractures, clouds, waves, etc. Different from Euclidean geometries that are smooth and continuous in general, fractals show irregularity and roughness. Yet the seemingly complex structures can be generated based on simple principles.

Fractals have been applied in designing porous structures. For instance, as shown in Fig. 1, micro radioelectric antennas with 2D fractal geometries have good multi-band performance and reconfigurability [1]. Nanoscale fractal optical sensors can be used for infra and multi-spectral imaging [2]. Fractals observed in porous silicon at microscale are closely related to the wavelength of visible photoluminescence in designing light-emitting diodes (LED) [3]. It is foreseen that porous structures with fractal geometries will be useful in product and materials design in the future, such as in the application domains of sensing, energy storage, and catalysis. How to construct 3D fractal geometries efficiently in computers then is important to design porosity.

In this paper, we use a recently proposed periodic surface model [4, 5] to construct 3D fractal geometries. The periodic surface model itself can generate porous and repetitive structures efficiently. Fractals based on periodic surfaces can further enhance porosity. Three construction approaches are proposed in this paper. By applying orthonormal mappings iteratively in the Euclidean or parameter space of periodic surfaces, we can build 3D fractals. In addition, we also studied the relationship between porosity and fractal dimension. Each fractal has an associated fractal dimension that characterizes the extension of irregularity. We can use porosity as a metric in fractal design in parallel with fractal dimension, as many applications such as antennas and censors require high surface volume ratios. Porosity is physically measurable and can be used to observe fractal dimensions.

The rest of the paper is organized as follows. A brief background introduction of fractals and periodic surface models is given in Sect. 2. In Sect. 3, three construction approaches for 3D fractals are described. In Sect. 4, we define porosity and show its relationship with the fractal dimension.

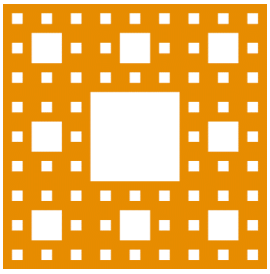

(a) 2D Sierpinski carpet antenna [1]

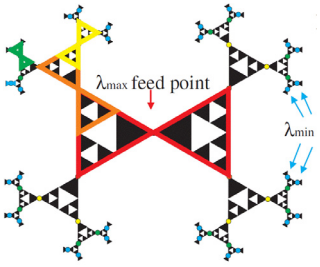

(b) Fractals for optical sensors [2]

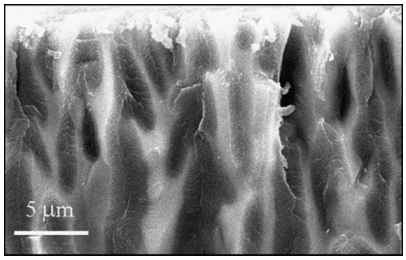

(c) Fractals in porous silicon for LED design [3]

Fig. 1: Fractals used in designing micro and nano structures

2. BACKGROUND

2.1 Fractal Geometry

Fractals [6] are irregular and fragmented geometries that exhibit self-similarity in different scales, where parts are reduced-size copies of the whole. Usually, a fractal has a simple and recursive definition. Yet its boundary is not smooth and cannot be represented in polynomials.

Fractal geometry could be generated by deterministic or random approaches. The iterated function system (IFS) is a generic way to do so [7,8]. An IFS is a finite collection of n functional mappings $F_i : \mathbb{R}^d \to \mathbb{R}^d \ (i = 1,\ldots,n)$ in the d-dimensional space, where the solution set $S \subset \mathbb{R}^d$ of the system is the fixed point of Hutchinson's recursive set equation [9]

$$S = \bigcup_{i=1}^{n} F_i(S) \tag{2.1}$$

Started from an initial position $\mathbf{x} \in \mathbb{R}^d$, fractals can be generated by applying Eqn.(2.1) iteratively. IFS should be selected such that it converges to a fixed point solution. S is also called *attractor* because typically $\|F_i(\mathbf{x}) - F_i(\mathbf{y})\| \le r\|\mathbf{x} - \mathbf{y}\|$ for any $\mathbf{x}, \mathbf{y} \in \mathbb{R}^d$, where r is a fixed number and called *dilation ratio*. For example, the Koch curve can be constructed with the IFS

$$F_i(x,y) = \begin{bmatrix} a_i & b_i & e_i \\ c_i & d_i & f_i \\ 0 & 0 & 1 \end{bmatrix} \begin{bmatrix} x \\ y \\ 1 \end{bmatrix} \quad (i = 1,2,3,4) \tag{2.2}$$

where the parameters $\begin{pmatrix} a_i & b_i & c_i & d_i & e_i & f_i \end{pmatrix}$'s are $\begin{pmatrix} 1/3 & 0 & 0 & 1/3 & 0 & 0 \end{pmatrix}$, $\begin{pmatrix} 1/6 & -\sqrt{3}/6 & \sqrt{3}/6 & 1/6 & 1/3 & 0 \end{pmatrix}$, $\begin{pmatrix} 1/6 & \sqrt{3}/6 & -\sqrt{3}/6 & 1/6 & 1/2 & 1/(2\sqrt{3}) \end{pmatrix}$, and $\begin{pmatrix} 1/3 & 0 & 0 & 1/3 & 2/3 & 0 \end{pmatrix}$. With two initial positions $[0,0]^T$ and $[1,0]^T$, the results up to five iterations are shown in Fig. 2.

A bounding shape B (e.g. box and sphere) includes the solution set, i.e. $S \subset B \subset \mathbb{R}^d$. For each non-overlapping subset of $S^{(j)}$ in iteration j, where $\bigcup_{j=1}^{N} S^{(j)} = S$ for a total of N iterations and $S^{(j_1)} \cap S^{(j_2)} = \varnothing$, there is also a subset of bounding shape $B^{(j)}$ such that $S^{(j)} \subset B^{(j)}$. The collection $\{B^{(j)}\}$ is also called a *δ-cover* of S if $S \subset \bigcup_j B^{(j)}$ and $0 < |B^{(j)}| \le \delta$ where $|B^{(j)}|$ is the *diameter* of $B^{(j)}$ defined as $|B^{(j)}| = \sup\{|\mathbf{x} - \mathbf{y}| : \forall \mathbf{x}, \mathbf{y} \in B^{(j)}\}$ where sup returns the supremum, which is also associated with scales.

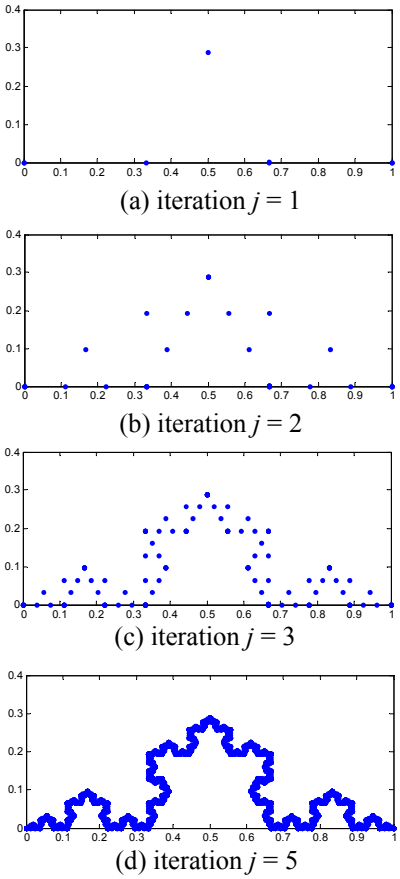

(a) iteration $j = 1$

(b) iteration $j = 2$

(c) iteration $j = 3$

(d) iteration $j = 5$

Fig. 2: The Koch curve generated with the IFS

Each fractal has a fractal dimension or Hausdorff dimension to characterize its extension of irregularity. The *Hausdorff measure* $\mathcal{H}_\delta^k(S)$ is the infimum of all δ-covers defined as $\mathcal{H}_\delta^k(S) = \inf\left\{\sum_{j=1}^{\infty} |B^{(j)}|^k\right\}$. And the *Hausdorff k-dimensional measure* is defined as $\mathcal{H}^k(S) = \lim_{\delta \to 0} \mathcal{H}_\delta^k(S)$. The *Hausdorff dimension* is thus defined as the infimum of the set of $D \in [0,\infty)$ such that the Hausdorff D-dimensional measure of spatial occupancy is zero. D can be estimated by solving $r_1^D + r_2^D + \cdots + r_N^D = 1$, where r_j is the dilation ratio associated the mapping in iteration j.

IFS can also be extended to stochastic models. Each function F_i has an associated probability. For each iteration, one of the n functions is chosen randomly to generate mappings. This is a Markov process which will converge to a stationary situation if one exists. Stochastic IFS's provide more flexibility and opportunities to create more interesting fractals than deterministic IFS's.

Fractal geometry has been studied extensively in the communities of mathematics, computer graphics, imaging processing and compression. IFS has been widely used to represent natural objects such as trees, plants, clouds, flames,

coast lines, and landscape. In geometric modeling domain, 2D and 3D fractal shapes have been demonstrated based on IFS's. However, most of the research was focused on point-based discrete modeling and rendering. Little was on parametric or implicit representations of geometries.

2.2 Fractals with Parametric and Implicit Modeling

Hart [10] introduced an implicit function based on an escape time $E(\mathbf{x})$, which is defined as the minimal number of inverse iterations in inverse functional mappings F_i^{-1} such that a point in the solution set S can "escape" the attraction and out of the bounding shape. The escape time is a function of location $\mathbf{x}$. A continuous version of the escape time function $E(\mathbf{x})$ [11] was used, and fractal surfaces are defined by $1/E(\mathbf{x})$, since $E(\mathbf{x})=\infty$ for $\mathbf{x}\in S$ and $E(\mathbf{x})\geq 0$ for $\mathbf{x}\notin S$.

Zair and Tosan [12] constructed fractal surfaces by defining IFS in the parametric domain such that parameters of Bézier and B-spline surfaces are fractals. The mapping from the parametric domain to Euclidean domain thus creates free-form fractal surfaces. Later, the approach was generalized to a control grid based subdivision scheme [13].

Different from the above, in this paper we present three 3D fractal construction methods based on a recently proposed periodic surface model. Periodic surfaces itself can model complex and porous structures efficiently. The implicit periodic boundary condition allows us to generate repetitive patterns effectively.

2.3 Periodic Surface (PS) Model

The periodic surface model has the implicit form and is defined as

$$\psi(\mathbf{r})=\sum_{l=1}^{L}\sum_{m=1}^{M}\mu_{lm}\cos\left(2\pi\kappa_l(\mathbf{p}_m^T\cdot\mathbf{r})\right)=0 \qquad (2.3)$$

where κ_l is the *scale parameter*, $\mathbf{p}_m=[a_m,b_m,c_m,d_m]^{\mathrm{T}}$ is a *basis vector*, such as one of

$$\{\mathbf{e}_0,\mathbf{e}_1,\mathbf{e}_2,\mathbf{e}_3,\mathbf{e}_4,\mathbf{e}_5,\mathbf{e}_6,\mathbf{e}_7,\mathbf{e}_8,\mathbf{e}_9,\mathbf{e}_{10},\mathbf{e}_{11},\mathbf{e}_{12},\mathbf{e}_{13},\ldots\}=$$

$$\left\{\begin{bmatrix}0\\0\\0\\1\end{bmatrix}\begin{bmatrix}1\\0\\0\\1\end{bmatrix}\begin{bmatrix}0\\1\\0\\1\end{bmatrix}\begin{bmatrix}0\\0\\1\\1\end{bmatrix}\begin{bmatrix}1\\1\\0\\1\end{bmatrix}\begin{bmatrix}1\\0\\1\\1\end{bmatrix}\begin{bmatrix}0\\1\\1\\1\end{bmatrix}\begin{bmatrix}1\\1\\1\\1\end{bmatrix}\begin{bmatrix}1\\-1\\0\\1\end{bmatrix}\begin{bmatrix}-1\\0\\1\\1\end{bmatrix}\begin{bmatrix}0\\1\\-1\\1\end{bmatrix}\begin{bmatrix}1\\-1\\1\\1\end{bmatrix}\begin{bmatrix}-1\\1\\1\\1\end{bmatrix}\begin{bmatrix}1\\1\\-1\\1\end{bmatrix}\cdots\right\} \qquad (2.4)$$

which represents a *basis plane* in the Euclidean space, $\mathbf{r}=[x,y,z,w]^{\mathrm{T}}$ is the location vector with homogeneous coordinates, and μ_{lm} is the *periodic moment*. We assume $w=1$ if not explicitly specified. We call $d_m=\mathbf{p}_m^{\mathrm{T}}\cdot\mathbf{r}/\|\mathbf{p}_m\|$ corresponding to the basis plane $\mathbf{p}_m$ as the *projective distance*. The degree of $\psi(\mathbf{r})$ in Eqn.(2.3) is defined as the number of unique vectors in the basis vector set $\{\mathbf{p}_m\}$. The scale of $\psi(\mathbf{r})$ is defined as the number of unique scale parameters in $\{\kappa_l\}$. We can assume scale parameters as natural numbers ($\kappa\in\mathbb{N}$).

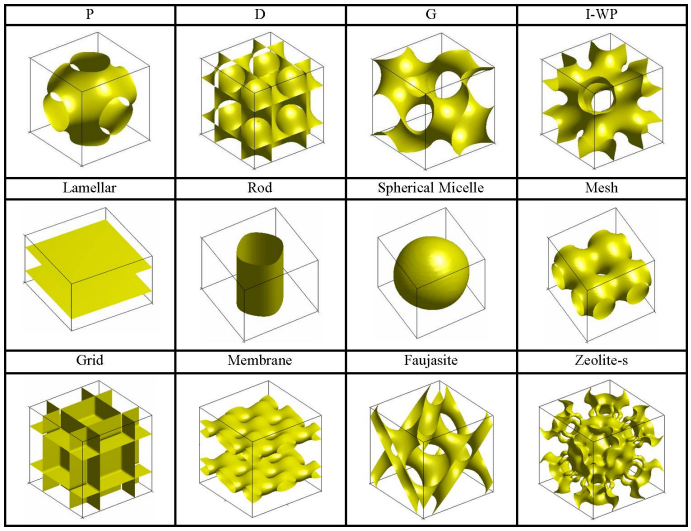

Fig. 3: Periodic surface models of cubic phase and mesophase structures

Fig. 3 lists some examples of periodic surface models. Triply periodic minimal surfaces, such as P-, D-, G-, and I-WP cubic morphologies that are frequently referred to in chemistry and polymer literature, can be adequately approximated. Besides the cubic phase, other mesophase structures such as spherical micelles, lamellar, rod-like hexagonal phases can also be modeled.

In this paper, we present three 3D fractal construction approaches using the periodic surface model. Periodic surfaces have the unique property of translational symmetry in all x, y, and z directions. This provides a convenient way to generate continuous and porous structures. Introducing fractals can further enhance porosity of these periodic structures. Uniform volume textures can be created.

3. 3D FRACTALS BASED ON PS MODELS

Self-similarity at different scales is an important property of fractals. A fractal object S is self-similar at different scales if the minimal overlap condition is satisfied, That is, $\bigcup_{i=1}^{n}F_i(S)\subset S$ and $F_i(S)\cap F_j(S)=\varnothing\ (\forall i\neq j)$ (or $\mathcal{H}^D\left(F_i(S)\cap F_j(S)\right)=0\ (\forall i\neq j)$), where F_i's are IFS mapping functions. Following the principle, we developed three approaches to construct 3D periodic fractals based on PS models and IFS. The first approach is called iterated cut, where 3D portions are removed iteratively. The second approach, called constructive IFS, accumulates 3D segments iteratively. The third approach is a generic way to create periodic rough surfaces where iterations occur in the parameter space of the PS model.

3.1 Iterated Cut

The first method to build 3D fractals is applying IFS in the material removal process. Fractals can have non-integer

dimensions because some portions of geometries are removed iteratively. This creates irregularity that cannot be observed in integer dimensional Euclidean geometries. A classical example is the Sierpinski carpet shown in Fig. 1-(a). In 3D space, the corresponding one is the Menger sponge.

Menger sponge (or Menger-Sierpinski sponge) is a 3D cubic structure, with each face as a Sierpinski carpet. Similar to the construction approach of Sierpinski carpet [6], we may build Menger sponge as follows. Starting with a cube (denoted as $M^{(0)}$), we divide it into a^3 equal-sized sub-cubes, where $a \geq 3$. Remove a symmetric pattern of b sub-cubes $m^{(0)}$ from $M^{(0)}$ and the remain is $M^{(1)} = M^{(0)} \setminus m^{(0)}$. Repeat the procedure on each of the remaining sub-cubes, by dividing into a^3 further smaller sub-cubes and removing the same symmetric pattern as before. This process can continue with an infinite number of steps. The final $M = \bigcap_{j=0}^{\infty} M^{(j)}$ is the Menger sponge. The Hausdorff dimension of M is $d_H = \log\left(a^3 - b\right)/\log a$.

Similarly, to build a 3D PS fractal model, we first generate the removed portion $T = \bigcup_{j=0}^{N} T^{(j)}$, where $T^{(j)}$ is recursively generated by the IFS E_i's as $T^{(j)} = \bigcup_{i=1}^{n} E_i\left(T^{(j-1)}\right)$. Then the final model is $V = V^{(\kappa^N)} \setminus T$, where $V^{(\kappa^N)} = \left\{\psi^{(\kappa^N)}(\mathbf{r}) \leq 0\right\}$ and $\psi^{(\kappa^N)}(\mathbf{r})$ denotes the PS model defined in Eqn.(2.3) but with the smallest scale in the cube subdivision. That is, by the IFS F_{κ_1}, $\psi^{(\kappa_1 \cdot \kappa_2)}(\mathbf{r}) = F_{\kappa_1}\left(\psi^{(\kappa_2)}(\mathbf{r})\right) = \psi^{(\kappa_2)}(\mathbf{K} \cdot \mathbf{r})$, where $\mathbf{K} = \mathrm{diag}\left(1/\kappa_1, 1/\kappa_1, 1/\kappa_1, 1\right)$ is a scaling matrix. The generic algorithm of the iterated cut is listed in Fig. 4. Notice that in implicit functions *min* is the union operation and *max* is the intersection.

Fig. 5 shows an example of Menger sponge P surface model of two iterations. The P surface is defined as

$$\psi_P = \cos(2\pi x) + \cos(2\pi y) + \cos(2\pi z) = 0 \qquad (3.1)$$

The Menger sponge PS model is created by replacing each of the sub-cubes by a periodic unit cell of the corresponding scale. For each iteration, the unit cell is divided into 64 equal-sized sub-cubes, 32 of which at the center of the body and centers of faces are removed. Then each of the remaining 32 sub-cubes is divided.

3.2 Constructive IFS

The second method to generate PS fractal models is a constructive approach. We can build 3D segments iteratively, and the final geometry is a union of them. Since PS models can fill up space globally, we apply a special window function $W_i(\mathbf{r})$, which defines boundaries of PS models and selects a domain W_i. Then only a specific portion $U_i^{(j)} = V^{(j)} \cap W_i^{(j)}$ $(i = 1, \ldots, n)$ is taken into consideration. The IFS $G_i : \mathbb{R}^4 \to \mathbb{R}^4$ is applied to W_i iteratively in the construction process. Therefore, $U^{(j)} = F\left(V^{(j-1)}\right) \cap \bigcup_{i=1}^{n} G_i\left(W^{(j-1)}\right)$. Then the final structure is $U = \bigcup_{j=1}^{N} U^{(j)}$. The general algorithm of the constructive IFS approach is listed in Fig. 6.

Fig. 7 shows an example of the constructive approach with the G surface as the basic building block. The G surface is defined as

$T = \infty$;
κ = scale ratio ;
For $j = 1$ to N
  $T^{(j)} = \infty$;
  For $i = 1$ to n
    $T_i^{(j)} = E_i\left(T^{(j-1)}\right)$;
    $T^{(j)} = \min\left(T^{(j)}, T_i^{(j)}\right)$;
  End
  $T = \min\left(T, T^{(j)}\right)$;
  $\kappa = \kappa \times \kappa$;
End
$V = \psi^{(\kappa)}(\mathbf{r})$;
$V = \max(V, -T)$;
Return V ;

Fig. 4: Iterated cut algorithm for PS fractal model generation

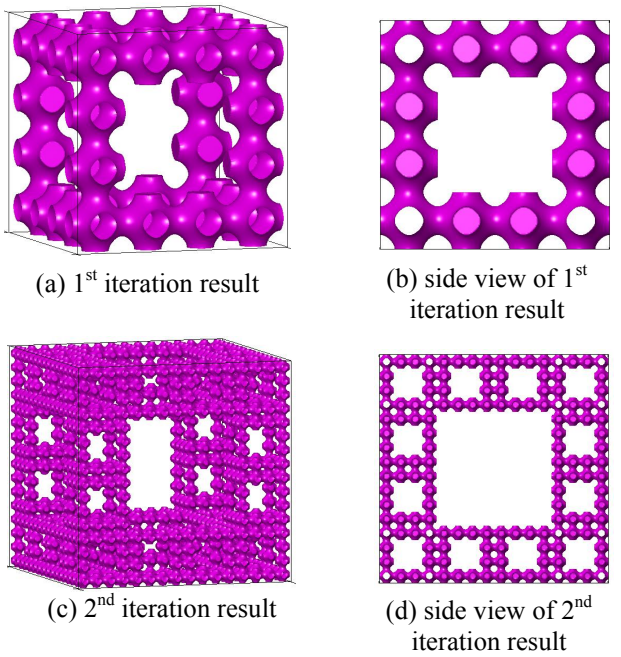

(a) 1st iteration result
(b) side view of 1st iteration result
(c) 2nd iteration result
(d) side view of 2nd iteration result

Fig. 5: A Menger sponge P surface model with $a = 4$ and $b = 32$

$U = \infty$;
κ = scale ratio ;
For $j = 1$ to N
  $W^{(j)} = \infty$;
  For $i = 1$ to n
    $W_i^{(j)} = G_i\left(W^{(j-1)}\right)$;
    $W^{(j)} = \min\left(W^{(j)}, W_i^{(j)}\right)$;
  End
  $V^{(j)} = \psi^{(\kappa)}(\mathbf{r})$;
  $U^{(j)} = \max\left(V^{(j)}, W^{(j)}\right)$;
  $U = \min(U, U^{(j)})$;
  $\kappa = \kappa \times \kappa$;
End
Return U ;

Fig. 6: The algorithm of the constructive IFS approach to generate 3D PS fractals

$$\begin{aligned}\psi_G &= \cos\left(2\pi\left(-x-y+.25\right)\right)+\cos\left(2\pi\left(-x+y+.25\right)\right)\\ &+\cos\left(2\pi\left(-y-z+.25\right)\right)+\cos\left(2\pi\left(-y+z+.25\right)\right)\\ &+\cos\left(2\pi\left(-x-z+.25\right)\right)+\cos\left(2\pi\left(x-z+.25\right)\right)\\ &= 0\end{aligned} \tag{3.2}$$

The two IFS functions for the windows are

$$G_1^{(j)}(x,y,z) = \begin{bmatrix} 1/2 & & & 3w_x^{(j-1)}/4 \\ & 1/2 & & w_y^{(j-1)}/4 \\ & & 1/2 & w_z^{(j-1)}/4 \\ & & & 1 \end{bmatrix} \begin{bmatrix} x \\ y \\ z \\ 1 \end{bmatrix}$$

and

$$G_2^{(j)}(x,y,z) = \begin{bmatrix} 1/2 & & & 3w_x^{(j-1)}/4 \\ & 1/2 & & -w_y^{(j-1)}/4 \\ & & 1/2 & -w_z^{(j-1)}/4 \\ & & & 1 \end{bmatrix} \begin{bmatrix} x \\ y \\ z \\ 1 \end{bmatrix}$$

where $w_x^{(j)}$, $w_y^{(j)}$ and $w_z^{(j)}$ are the width of the window in x, y and z directions respectively at iteration j. The IFS function F for PS model ψ_G is simply a scaling matrix with a factor of 2. Fig. 8 shows another example of construction model with the P surface defined in Eqn.(3.1) as the building block. It has twelve IFS G_i's corresponding to the window function. The IFS function for the P surface model is a scaling matrix with the factor of 3.

3.3 Periodic Rough Surfaces

Rough surfaces such as rocks and landscape have been modeled as fractals. The one in Fig. 1-(c) is another example. The third approach in construction of periodic fractals is to apply IFS's in the parameter space of PS models. The parameter space of PS models is the one where the basis vectors $\mathbf{p}_m$'s and moments μ_{lm}'s are defined as in Eqn.(2.3). We can define the IFS $H_i : \mathbb{R}^4 \to \mathbb{R}^4$ $(i = 1,\ldots,n)$ as an orthonormal transformation matrix (such as scaling, rotation, translation). For a PS model with a set of basis vectors $\{\mathbf{p}_m\}$, we may rewrite them in the matrix form as

$$P^{(0)} = \begin{bmatrix} \mathbf{p}_1 & \cdots & \mathbf{p}_M \end{bmatrix} \tag{3.3}$$

By applying the matrix H_i iteratively as in

$$P^{(j)} = \bigcup_{i=1}^{n} H_i P^{(j-1)} \tag{3.4}$$

we receive a series of basis vectors which themselves exhibit fractal patterns in the parameter P-space. In addition, we also define a scaling factor s for the collection of moments $\mathrm{M} = \{\mu_{lm}\}$ as in

$$\mathrm{M}^{(j)} = s\mathrm{M}^{(j-1)} \tag{3.5}$$

By evaluating Eqn.(2.3) with all basis vectors $\bigcup_{j=1}^{N} P^{(j)}$ and moments $\bigcup_{j=1}^{N} \mathrm{M}^{(j)}$, we can generate periodic rough surfaces in the Euclidean space.

As an example, we add fractal patterns to an F (Faujasite) surface defined as

$$\begin{aligned}\psi_F &= -0.50992 - 0.0098336\cos\left(2\pi x\right) - 0.0098336\cos\left(2\pi y\right)\\ &-0.0098336\cos\left(2\pi z\right) - 0.0042982\cos\left(2\pi\left(x+y\right)\right)\\ &-0.0042982\cos\left(2\pi\left(x+z\right)\right) - 0.0042982\cos\left(2\pi\left(y+z\right)\right)\\ &-0.015304\cos\left(2\pi\left(x-y\right)\right) - 0.015304\cos\left(2\pi\left(z-x\right)\right)\\ &-0.015304\cos\left(2\pi\left(y-z\right)\right) - 0.45206\cos\left(2\pi\left(x+y+z\right)\right)\\ &+0.42213\cos\left(2\pi\left(x-y+z\right)\right) + 0.42213\cos\left(2\pi\left(-x+y+z\right)\right)\\ &+0.42213\cos\left(2\pi\left(x+y-z\right)\right)\\ &= 0\end{aligned}$$

as shown in Fig. 9-(a). The IFS matrices applied in the parameter space are

$$H_1 = \begin{bmatrix} \lambda\cos\frac{\pi}{3} & -\lambda\sin\frac{\pi}{3} & 0 & 0 \\ \lambda\sin\frac{\pi}{3} & \lambda\cos\frac{\pi}{3} & 0 & 0 \\ 0 & 0 & 1 & 0 \\ 0 & 0 & 0 & 1 \end{bmatrix} \tag{3.6}$$

and

$$H_2 = \begin{bmatrix} \lambda\cos\frac{\pi}{3} & \lambda\sin\frac{\pi}{3} & 0 & 0 \\ -\lambda\sin\frac{\pi}{3} & \lambda\cos\frac{\pi}{3} & 0 & 0 \\ 0 & 0 & 1 & 0 \\ 0 & 0 & 0 & 1 \end{bmatrix} \tag{3.7}$$

where the P-space scaling factor $\lambda = 10$. Notice that the basis vectors are in the reciprocal space. Any scaling factor $\lambda > 1$

increases the frequencies. The effect of the IFS H_1 and H_2 is that vectors are scaled up and rotated iteratively. The fractal patterns of basis vectors in the P-space are shown in Fig. 10. Fig. 10-(a) plots the original vectors of the F surface in the reciprocal space. Fig. 10-(b), -(c), and -(d) show the resultant basis vectors of IFS's after one, three, and ten iterations respectively. It can be seen that the similar pattern repeats itself at difference scales.

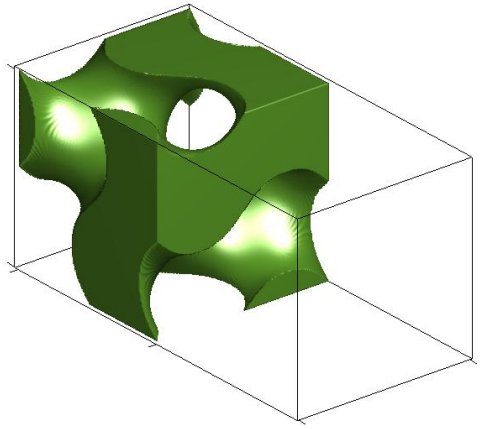

(a) Original G model

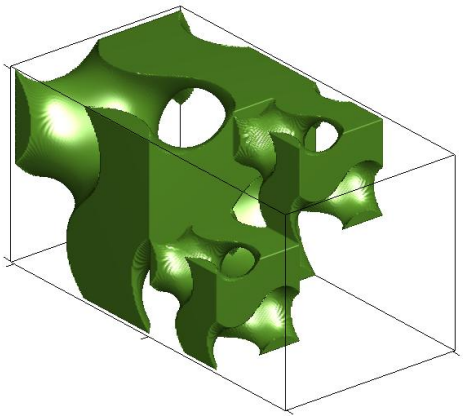

(b) G fractal with 1 iteration

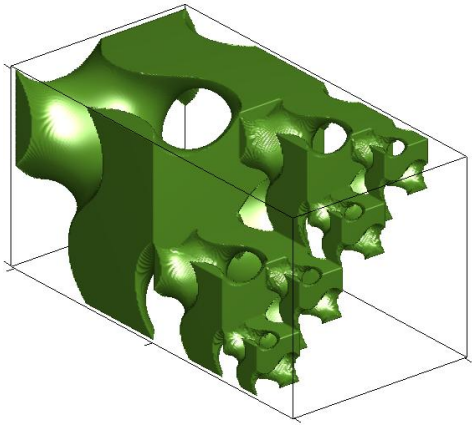

(c) G fractal with 2 iterations

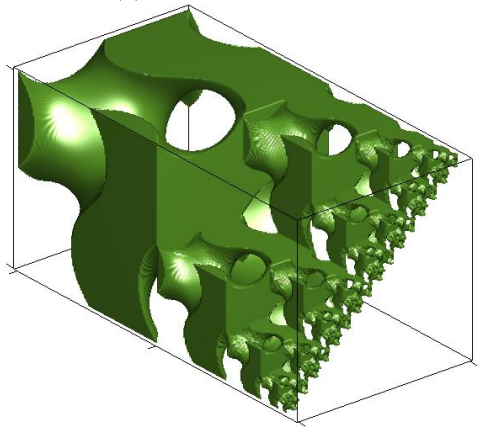

(d) G fractal with 4 iterations

Fig. 7: G fractals constructed from G surfaces

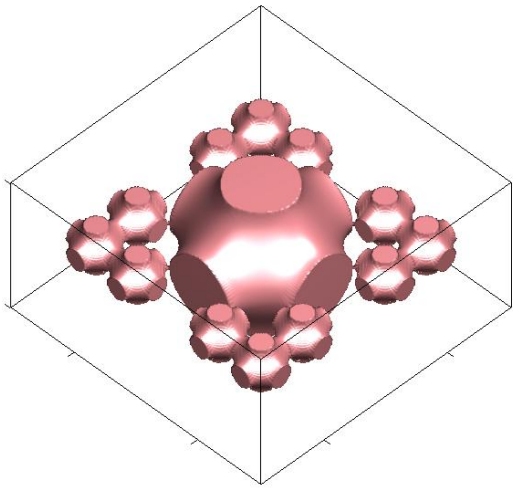

(a) P fractal with 1 iteration

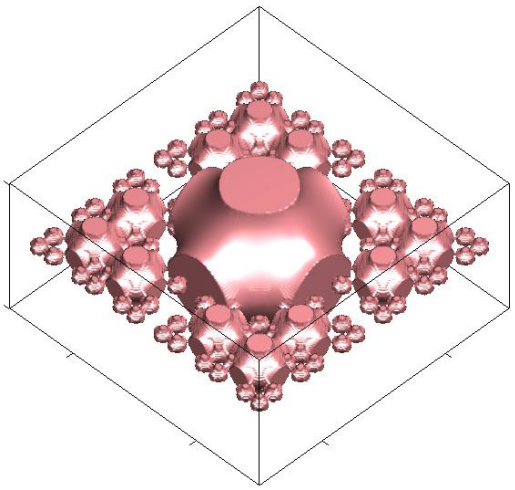

(b) P fractal with 2 iterations

Fig. 8: P fractals constructed from P surfaces

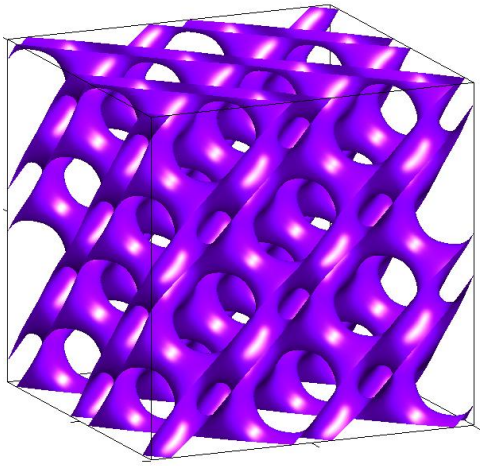

(a) Original F surface model

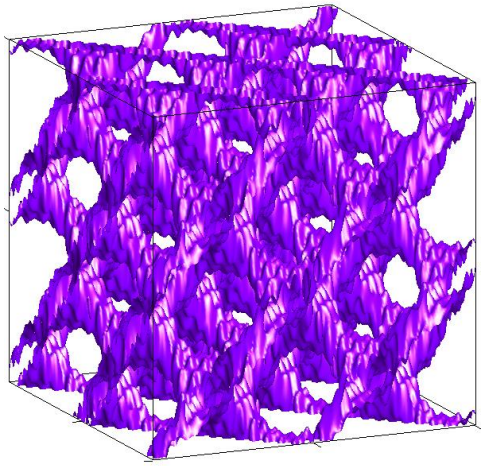

(b) F fractal with s=10 (1 iteration)

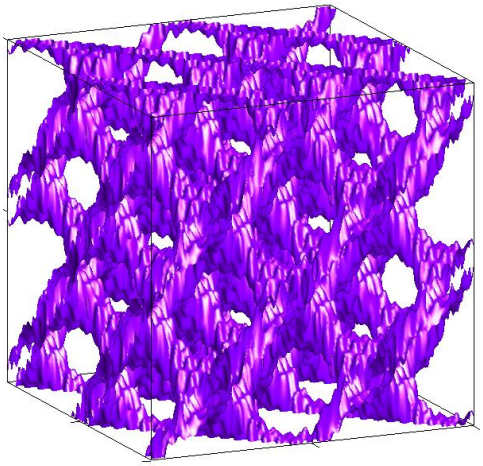

(c) F fractal with s=10 (3 iterations)

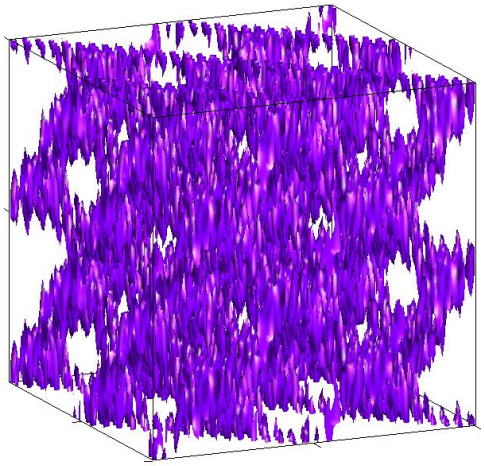

(d) F fractal with s=2 (1 iteration)

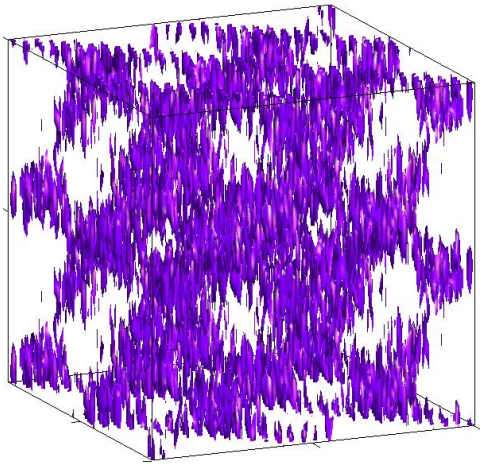

(e) F fractal with s=2 (3 iterations)

Fig. 9: F fractals constructed from IFS's in the basis vector parameter space.

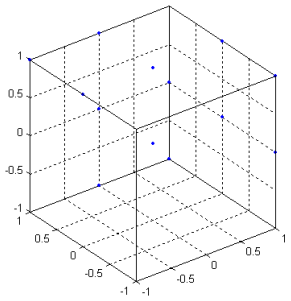

(a) Original basis vectors in *P*-space

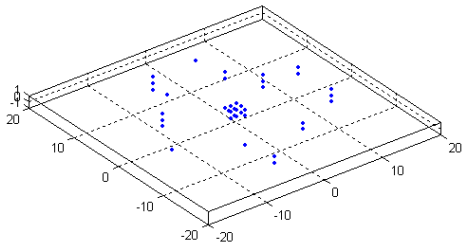

(b) Basis vector fractal in *P*-space (1 iteration)

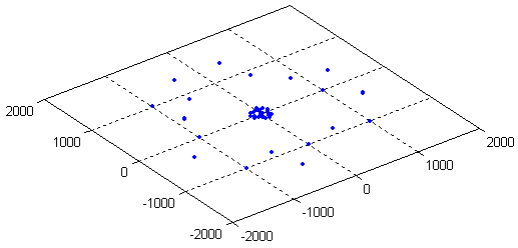

(c) Basis vector fractal in *P*-space (3 iterations)

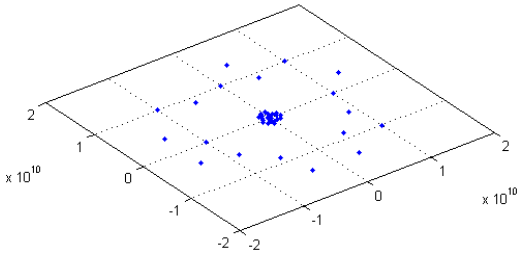

(d) Basis vector fractal in *P*-space (10 iterations)

Fig. 10: Basis vector fractals in *P*-space with IFS's in Eqns.(3.6) and (3.7) and λ=10.

For each iteration, a new set of basis vectors $\mathbf{p}_m$'s as in Eqn.(3.4) are generated, and the corresponding new moments μ_{lm}'s are the old ones multiplied by a M-space scaling factor s as in Eqn.(3.5). Then new terms are appended to old ones and a new PS model is formed. By applying different scaling factors s's, we observe different effects in the Euclidean space. As shown in Fig. 9-(b) and -(c), the M-space scaling factor is $s = 10$. The values of moments in additional terms reduce quickly. In Fig. 9-(d) and -(e), a smaller M-space scaling factor $s = 2$ gives a different roughness effect.

4. FRACTAL POROSITY

In the traditional geometric design, curvature is often used to evaluate smooth curves and surfaces. It also corresponds to acceleration, energy changes, etc. in physics. Similarly in design of non-smooth and irregular shapes of fractals, easy to measure and physically meaningful metrics are needed. Porosity is a natural choice of such metrics.

In [5], we defined porosity as

$$\phi = \frac{\iiint_{\mathbf{r}\in\mathbb{D}} \left(\psi(\mathbf{r}) / \psi_M\right)^2 d\mathbf{r}}{\iiint_{\mathbf{r}\in\mathbb{D}} d\mathbf{r}} \qquad (4.1)$$

to quantify the PS surface density within a domain $\mathbb{D}$, where $\psi_M = \max_{\mathbf{r}\in\mathbb{D}} \left(\left| \psi(\mathbf{r}) \right| \right)$.

For PS fractals, if a domain or cube is divided into A equal-sized sub-cubes and a symmetric pattern of b sub-cubes are replaced by a second type of model with the porosity of ϕ_b, we can define a *fractal porosity* at the j^{th} iteration as

$$\phi^{(j)} = \left(1 - \frac{b}{A}\right)\phi^{(j-1)} + \frac{b}{A}\phi_b^{(j-1)} \qquad (4.2)$$

where the porosity of models at the initial step $\phi^{(0)}$ is defined as in Eqn.(4.1). The porosity of an *empty cube* is defined as 1. Notice that porosity in Eqn.(4.1) is scale-invariant. The value of fractal porosity $\phi^{(j)}$ is always between $\phi^{(j-1)}$ and $\phi_b^{(j-1)}$.

The fractal porosity is closely related to the Hausdorff dimension when materials are always removed and replaced by b empty sub-cubes in each iteration. The smaller the Hausdorff dimension is, the greater the fractal porosity is. Because if $v = b / A$ is looked as the material removal ratio, a higher value of v corresponds to a lower value of Hausdorff dimension. The value of $\partial\phi^{(j)} / \partial v = \phi_b^{(j-1)} - \phi^{(j-1)} = 1 - \phi^{(j-1)}$ is always between 0 and 1 in the material removal cases where empty sub-cubes are applied. Therefore, the fractal porosity is a monotone metric with respect to the Hausdorff dimension for a particular $\phi^{(0)}$ in the material removal cases.

Table 1 lists some fractal porosities of the examples in Section 3. For instance, the porosity of the Menger sponge P-fractal $\phi^{(0)} = 0.1667$ is calculated based on Eqn.(4.1). The following $\phi^{(1)}$ and $\phi^{(2)}$ are calculated based on Eqn.(4.2). Those for F-fractals in Fig. 9 are calculated only based on Eqn.(4.1).

Table 1: Values of fractal porosity in the examples of Section 3

	Menger Sponge P fractal (Fig. 5)	G fractal (Fig. 7)	P fractal (Fig. 8)	F surface (Fig. 9)	F fractal s=10 (Fig. 9)	F fractal s=2 (Fig. 9)
$\phi^{(0)}$	0.1667	0.6667	0.9074	0.2066	0.2066	0.2066
$\phi^{(1)}$	0.5834	0.5833	0.8663		0.1805	0.1418
$\phi^{(2)}$	0.7917	0.5625	0.8607		0.1781	0.1491

5. SUMMARY

In this paper, we presented 3D fractal construction approaches using the periodic surface model. With the repetitive and porous properties of the implicit surface model, irregular geometries at different scales can be constructed efficiently. A new scale invariant metric, fractal porosity, is also proposed to assess 3D fractals and porosity design in parallel with the Hausdorff dimension.

The goal of the paper is to explore the potentials of PS models in fractal modeling to design porous structures. Further sensitivity studies of both PS models and the metric of porosity are necessary to understand how to control structural variations if parameters are modified. Interesting questions, such as how PS fractals provide different effects compared to other fractals, how porosity and the Hausdorff dimension can be used as tools and guidance in building fractals for specific design needs, and many others still need to be answered.

ACKNOWLEDGEMENT

This work is supported in part by the NSF grant CMMI-1001040.

REFERENCES

[1] Werner, D.H.; Ganguly, S. (2003) An overview of fractal antenna engineering research. *IEEE Antennas & Propagation Magazine*, **45**(1): 38-57.

[2] Alda, J., Rico-García, J.M., López-Alonso, J.M. and Boreman, G. (2005) Optical antennas for nano-photonic applications. *Nanotechnology*, **16**(5): S230-S234

[3] Huang, Y.M., Zhai, B., and Zhou, F. (2008) Correlation of excitation-wavelength dependent photoluminescence with the fractal microstructures of porous silicon. *Applied Surface Science*, **254**(13): 4139-4143.

[4] Wang, Y. (2007) Periodic surface modeling for computer aided nano design. *Computer-Aided Design*, **39**(3): 179-189.

[5] Wang, Y. (2007) Loci periodic surface reconstruction from crystals. *Computer-Aided Design & Applications*, **4**(1-4): 437-447.

[6] Mandelbrot, B.B. (1983) *The Fractal Geometry of Nature*, W.H. Freeman, New York.

[7] Demko, S.; Barnsley, M. F. (1985) Iterated function systems and the global construction of fractals. *Proc. Royal Society of London*, **A399**(1817): 243-275.

[8] Demko, S., Hodges, L., Naylor, B. (1985) Construction of fractal objects with iterated function systems. *Proc. SIGGRAPH 1985*, **19**(3): 271-278.

[9] Hutchinson, J.E. (1981) Fractals and self-similarity. *Indiana University Mathematics Journal*, **30**(5): 713-747.

[10] Hart, J.C. (1997) Implicit representation of rough surfaces. *Computer Graphics Forum*, **16**(2): 91-99.

[11] Hepting, D., Prusinkiewicz, P., and Saupe, D. (1990) Rendering methods for iterated function systems. *Proc. IFIP Fractals'90*.

[12] Zair, C.E. and Tosan, E. (1996) Fractal modeling using free form techniques. *Computer Graphics Forum*, **15**(3): 269-278.

[13] Guérin, E., Tosan, E., and Baskurt, A. (2001) Fractal approximation of surfaces based on projected IFS attractors. *Proc. EUROGRAPHICS 2001*.